

# *Moisture sources for East Asian precipitation: mean seasonal cycle and interannual variability*

Article

Published Version

Open Access

Guo, L., van der Ent, R., Klingaman, N. ORCID: <https://orcid.org/0000-0002-2927-9303>, Demory, M.-E., Vidale, P. L. ORCID: <https://orcid.org/0000-0002-1800-8460>, Turner, A. ORCID: <https://orcid.org/0000-0002-0642-6876>, Stephan, C. and Chevuturi, A. ORCID: <https://orcid.org/0000-0003-2815-7221> (2019) Moisture sources for East Asian precipitation: mean seasonal cycle and interannual variability. *Journal of Hydrometeorology*, 20. pp. 657-672. ISSN 1525-7541 doi: <https://doi.org/10.1175/JHM-D-18-0188.1> Available at <https://centaur.reading.ac.uk/82517/>

It is advisable to refer to the publisher's version if you intend to cite from the work. See [Guidance on citing](#).

To link to this article DOI: <http://dx.doi.org/10.1175/JHM-D-18-0188.1>

Publisher: American Meteorological Society

All outputs in CentAUR are protected by Intellectual Property Rights law, including copyright law. Copyright and IPR is retained by the creators or other copyright holders. Terms and conditions for use of this material are defined in the [End User Agreement](#).

[www.reading.ac.uk/centaur](http://www.reading.ac.uk/centaur)

**CentAUR**

Central Archive at the University of Reading

Reading's research outputs online

## Moisture Sources for East Asian Precipitation: Mean Seasonal Cycle and Interannual Variability

LIANG GUO

*National Centre for Atmospheric Science, Department of Meteorology, University of Reading, Reading, United Kingdom*

RUUD J. VAN DER ENT

*Department of Water Management, Faculty of Civil Engineering and Geosciences, Delft University of Technology, Delft, and Department of Physical Geography, Faculty of Geosciences, Utrecht University, Utrecht, Netherlands*

NICHOLAS P. KLINGAMAN, MARIE-ESTELLE DEMORY, AND PIER LUIGI VIDALE

*National Centre for Atmospheric Science, Department of Meteorology, University of Reading, Reading, United Kingdom*

ANDREW G. TURNER

*National Centre for Atmospheric Science, Department of Meteorology, and Department of Meteorology, University of Reading, Reading, United Kingdom*

CLAUDIA C. STEPHAN AND AMULYA CHEVUTURI


*National Centre for Atmospheric Science, Department of Meteorology, University of Reading, Reading, United Kingdom*

(Manuscript received 4 September 2018, in final form 14 January 2019)

### ABSTRACT

This study investigates the moisture sources that supply East Asian (EA) precipitation and their interannual variability. Moisture sources are tracked using the Water Accounting Model-2layers (WAM-2layers), based on the Eulerian framework. WAM-2layers is applied to five subregions over EA, driven by the ERA-Interim reanalysis from 1979 to 2015. Due to differences in regional atmospheric circulation and in hydrological and topographic features, the mean moisture sources vary among EA subregions. The tropical oceanic source dominates southeastern EA, while the extratropical continental source dominates other EA subregions. The moisture sources experience large seasonal variations, due to the seasonal cycle of the EA monsoon, the freeze–thaw cycle of the Eurasian continent, and local moisture recycling over the Tibetan Plateau. The interannual variability of moisture sources is linked to interannual modes of the coupled ocean–atmosphere system. The negative phase of the North Atlantic Oscillation increases moisture transport to northwestern EA in winter by driving a southward shift in the midlatitude westerly jet over the Mediterranean Sea, the Black Sea, and the Caspian Sea. Atmospheric moisture lifetime is also reduced due to the enhanced westerlies. In summers following El Niños, an anticyclonic anomaly over the western North Pacific increases moisture supplied from the South China Sea to the southeastern EA and shortens the traveling distance. A stronger Somali Jet in summer increases moisture to the Tibetan Plateau and therefore increases precipitation over the eastern Tibetan Plateau. The methods and findings in this study can be used to evaluate hydrological features in climate simulations.

---

 Denotes content that is immediately available upon publication as open access.

---

 Supplemental information related to this paper is available at the Journals Online website: <https://doi.org/10.1175/JHM-D-18-0188.s1>.

---

*Corresponding author:* Liang Guo, [l.guo@reading.ac.uk](mailto:l.guo@reading.ac.uk)

DOI: 10.1175/JHM-D-18-0188.1

© 2019 American Meteorological Society. For information regarding reuse of this content and general copyright information, consult the [AMS Copyright Policy \(www.ametsoc.org/PUBSReuseLicenses\)](https://www.ametsoc.org/PUBSReuseLicenses).

## 1. Introduction

East Asia (EA) is one of the most populated areas in the world. Understanding and predicting EA precipitation is essential for agriculture and socioeconomic development. East Asia is located over the eastern part of the Eurasian continent, spanning from the tropics to the temperate zones; its precipitation is linked to oceanic and terrestrial moisture sources across these regions. EA precipitation varies over time due to natural variability and human impacts, which can lead to extreme events such as drought and floods. To improve our understanding and prediction of EA precipitation, it is essential to identify its sources of moisture and their associated variability.

The climatology of EA precipitation decreases from southeast to northwest (Zhai et al. 2005). In winter, variations in moisture transport and precipitation over EA are dominated by the winter monsoon in the north and ENSO in the south. The EA winter monsoon is linked to the Arctic Oscillation (AO) and the intensity of the Siberian High (Gong and Ho 2002; Gong et al. 2001; Wu et al. 2010). Wang et al. (2000) showed that precipitation variability over southern China in winter is linked to ENSO. During El Niño in the eastern Pacific, an anomalous low-level anticyclone in the western North Pacific weakens the EA winter monsoon and increases precipitation over southern China. In summer, the interannual variability of precipitation and moisture transport is also dominated by ENSO (Huang and Wu 1989; Wang et al. 2003; Xie et al. 2009). Because of the abundance of precipitation over the southeast, most previous studies focused on identifying moisture sources for this subregion (Ding and Chan 2005; Baker et al. 2015; Pan et al. 2017; Sun and Wang 2015; Li et al. 2013; Chu et al. 2017). As the EA summer monsoon dominates the seasonal cycle of this subregion, previous studies agree that the major moisture sources for southeast EA precipitation are oceanic.

Northern and western EA have not gained as much attention as southeastern EA. However, as pointed out by the Fifth Assessment Report of the United Nations Intergovernmental Panel on Climate Change (IPCC AR5; Seneviratne et al. 2012), these subtropical and midlatitude land regions may experience a drying trend under a warmer climate, with increasing risks of drought and heavy rainfall. Existing studies focused on different subregions, for example, the semiarid grasslands (Sun and Wang 2014), northeast China (Simmonds et al. 1999), and the Chinese Loess Plateau (Hu et al. 2018). The dominant moisture source in each case is continental. These results are supported by global studies. For example, by studying the origin and fate of atmospheric moisture over continents, van der Ent et al.

(2010) pointed out that northern China is a sink of moisture that originates from the Eurasian continent. Recent studies further revealed that, even for southeastern EA, where oceanic moisture sources dominate, contributions from tropical land cannot be neglected (Wei et al. 2012; Zhao et al. 2016). On the other hand, local sources of moisture may be important for Tibet, as the Himalayas block moisture originating from the Indian Ocean and prevent local moisture from being advected out of the region, resulting in a high local moisture recycling ratio (van der Ent et al. 2010; Zhang et al. 2017a; Curio et al. 2015).

Guo et al. (2018) investigated local and remote moisture sources across EA. Considering the inhomogeneity of EA precipitation, EA was divided into five more homogeneous subregions according to hydrological features and topography. The hydrological cycle and moisture sources were compared between these regions. The authors attributed EA precipitation to local evaporation as well as remote moisture influxes from different directions. However, they could not identify remote moisture sources region due to the limits of their analytical method.

In this study, we identify sources of moisture for precipitation across EA using the Water Accounting Model-2layers (WAM-2layers; van der Ent et al. 2013). WAM-2layers is an Eulerian tracking method. An advantage over previous Eulerian methods is that WAM-2layers is able to trace atmospheric moisture to its origin or destination. WAM-2layers has been applied to track moisture for various regions, from small regions to entire continents, including Africa, Asia, and Europe (van der Ent et al. 2010; Keys et al. 2014; Zhang et al. 2017a). Results from these studies are consistent with studies using other tracking methods. A description of WAM-2layers is given in section 2b; comparisons between WAM-2layers and other tracking methods are made in section 5.

Using WAM-2layers, Keys et al. (2014) pointed out that the domains of the moisture source regions show little interannual variability for precipitation over the western Sahel, northern China, and the La Plata basin. The authors defined a core source region as a region with a contribution to precipitation above a chosen threshold every year. The interannual variation of regional precipitation, therefore, is explained by changes in evaporation intensity from the core source region. However, based on empirical orthogonal function analysis, Keys et al. (2014) also pointed out that the interannual variability in moisture source regions shows dipole patterns associated with oscillations in large-scale climate phenomena, for example, El Niño–Southern Oscillation (ENSO) or other sea surface temperature (SST) variations. This result is consistent with previous studies that investigated the relationship between atmospheric circulation and moisture fluxes (Zhou and Yu

2005; Li and Zhou 2012; Stephan et al. 2018; Guo et al. 2018). However, Keys et al. (2014) did not study the physical mechanisms underlying this response.

In this study, the moisture sources for EA precipitation will be traced and compared across EA by dividing it into five subregions. Contributions from different sources will be calculated and compared on annual and seasonal scales. The relationship between moisture sources, atmospheric circulation, and EA precipitation on interannual time scales will also be investigated. The method and data will be described section 2. Section 3 discusses the moisture sources for seasonal and annual EA precipitation, while section 4 discusses their interannual variation. A discussion and summary are given in sections 5 and 6, respectively.

## 2. Data and methods

### a. Data

The European Centre for Medium-Range Weather Forecasts interim reanalysis dataset (ERA-Interim) for 1979–2015 (Berrisford et al. 2011; Dee et al. 2011) is used in this study. Variables used include precipitation and total surface evaporation, the horizontal winds, and specific humidity on model levels, and the vertically integrated moisture flux. All variables are 6-hourly data and gridded on a  $1.5^\circ \times 1.5^\circ$  regular grid, except for precipitation and evaporation, which are 3-hourly accumulated data. Trenberth et al. (2011) pointed out that the global hydrological budget is not closed in many reanalyses datasets, due to the analysis increment applied by the data assimilation scheme. Our choice of ERA-Interim is justified on the basis that the residual in the global hydrological budget is the smallest among

reanalyses (Trenberth et al. 2011). ERA-Interim also shows the highest fidelity among reanalyses in terms of reproducing the mean and interannual variability of EA monsoon precipitation (Lin et al. 2014). ERA-Interim produces a reasonable estimate of evaporation over China in both spatial pattern and interannual variability, compared to observations (Su et al. 2015).

### b. Water Accounting Model-2layers

WAM-2layers was described by van der Ent et al. (2013, 2014) based on the atmospheric water conservation equation. WAM-2layers is an offline moisture tracking method based on the Eulerian framework. The accuracy of WAM-2layers was significantly improved in van der Ent et al. (2013) by expanding the previous single-layer WAM (van der Ent et al. 2010) into a two-layer model that considers the vertical shear of the moisture flux.

WAM-2layers combines data for precipitation, evaporation, atmospheric circulation, and moisture to determine the sources or sinks of moisture for a study region from a chosen domain (either globally or regionally). A critical output from WAM-2layers for our study is the tracked evaporation, defined as evaporation from any grid point that becomes precipitation in the region under study. Based on this variable, the source region can be defined, which is the domain wherein the sum of the tracked evaporation is equal to the precipitation in the study region.

Apart from the tracked evaporation, WAM-2layers also has a tracer to measure the lifetime of atmospheric moisture as it travels from source to sink. At each time step  $t$ , the model calculates the lifetime of the tracked moisture at that location according to Eq. (1) of van der Ent and Tuinenburg (2017),

$$N_g^t = \frac{1}{W_g^t} \times \left[ \underbrace{W_g^{t-1}(N_g^{t-1} + \Delta t)}_{\text{remaining vapor}} + \underbrace{\sum F_{g,\text{in}} \Delta t (N_{g,\text{in}}^{t-1} + \Delta t)}_{\text{influx}} - \underbrace{\sum F_{g,\text{out}} \Delta t (N_g^{t-1} + \Delta t)}_{\text{outflux}} - \underbrace{E_g \Delta t (N_g^{t-1} + \Delta t)}_{\text{evaporation}} + \underbrace{P_g \Delta t \frac{\Delta t}{2}}_{\text{precipitation}} \right], \tag{1}$$

where the subscript  $g$  stands for tracked water;  $N_g^t$  is the lifetime of the tracked water in a grid cell at time step  $t$ ;  $W_g^t$  is the tracked water storage in a grid cell at time step  $t$ ;  $F_{g,\text{in}}$  and  $F_{g,\text{out}}$  are the influx and outflux the over boundaries of a grid cell, respectively; and  $E_g$  and  $P_g$  are the tracked evaporation and precipitation, respectively.

For backward tracking,  $E_g$  depletes aged water and  $P_g$  adds new water to a grid cell.

In this study, we developed a new tracer to measure the distance traveled by atmospheric moisture between source and sink. At each time step  $t$ , the model calculates the traveling distance of the tracked moisture in a grid cell as

$$D_g^t = \frac{1}{W_g^t} \times \left[ \underbrace{W_g^{t-1} D_g^{t-1}}_{\text{remaining vapor}} + \underbrace{\sum F_{g,\text{in}} \Delta t (D_{g,\text{in}}^{t-1} + \Delta d)}_{\text{influx}} - \underbrace{\sum F_{g,\text{out}} \Delta t D_g^{t-1}}_{\text{outflux}} - \underbrace{E_g \Delta t D_g^{t-1}}_{\text{evaporation}} \right], \tag{2}$$

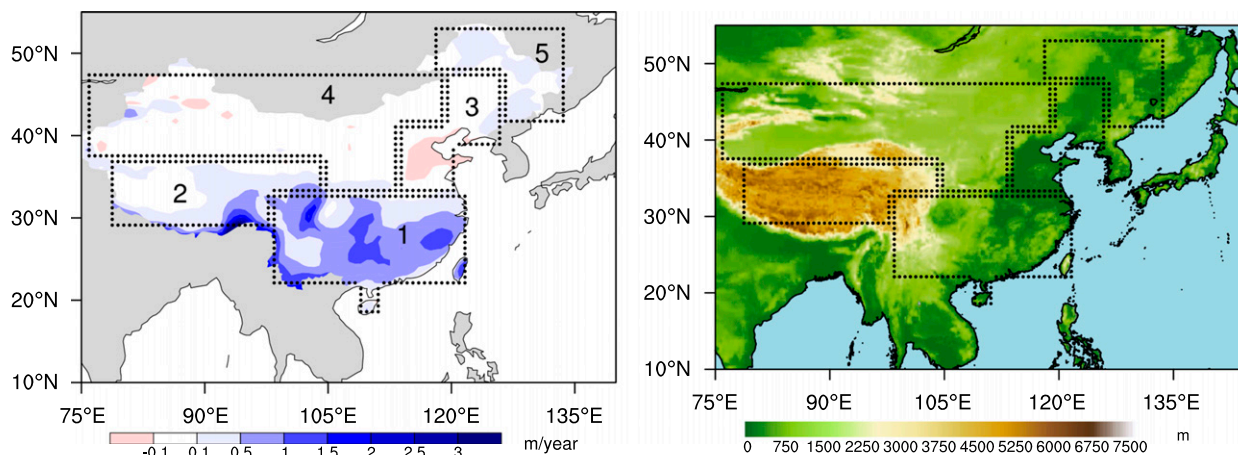


FIG. 1. (left) Annual mean precipitation minus evaporation ( $P - E$ ), calculated using the ERA-Interim reanalysis during 1979–2015 ( $\text{m yr}^{-1}$ ). (right) Topography over the EA landmass (m). Boxes 1–5 in the left panel indicate subregions over EA. This is reproduced from Guo et al. (2018).

where  $D_g^t$  is the traveling distance of the tracked water in a grid cell at time step  $t$ . Equation (2) is similar to Eq. (1) but with two differences. First, the distance will change only if moisture enters from another grid cell [i.e., the influx term in Eq. (2)]. Second, the distance for the new water is zero. For backward tracking, this means that the term related to the precipitation in Eq. (2) can be ignored. These tracers will help us to diagnose how moisture travels through the atmosphere, and therefore to build the physical link from source to sink.

EA crosses several climatic zones. To study its hydrological cycle, EA is first divided into smaller regions that are relatively homogeneous in terms of their hydrological features. To keep the number of regions manageable, we identify five regions according to precipitation minus evaporation ( $P - E$ ) and orography, as shown in Fig. 1. These regions are southeastern EA (SE, region 1), Tibetan Plateau (TP, region 2), central-eastern EA (CE, region 3), northwestern EA (NW, region 4), and northeastern EA (NE, region 5). The same division was used in Guo et al. (2018), wherein more discussion about this division and its comparison to previous divisions over EA can be found.

### 3. Annual and seasonal mean of moisture sources for EA precipitation

#### a. Annual mean

The annual mean moisture sources for precipitation in EA subregions are shown in Fig. 2. To compare differences between five EA subregions, we calculate the contributions of moisture from different sources. First, moisture sources are separated into tropics and extratropics (the

solstice latitudes,  $23.4^\circ\text{N}$  and  $23.4^\circ\text{S}$ , are used to separate the tropics and extratropics), as well as into land and sea, thereby delineating contributions into tropical sea  $T_s$ , tropical land  $T_l$ , extratropical sea  $X_s$ , and extratropical land  $X_l$ . The contribution from local evaporation (or the precipitation recycling ratio  $\rho$ ) is a separated fifth category. The annual contributions from these categories are listed in Table 1. The primary moisture source for region 1 (SE) is  $T_s$  (50%); the secondary source is  $\rho$  (16%). The primary moisture source for regions 2 (TP) and 3 (CE) is  $X_l$  (37% and 45%); the secondary source is  $T_s$  (24% and 28%). The oceanic moisture for region 3 (CE) originates from both the Indian and Pacific, while the oceanic moisture for region 2 (TP) originates only from the Indian Ocean (Figs. 2b,c). The primary moisture source for regions 4 (NW) and 5 (NE) is  $X_l$  (53% and 58%); the secondary is  $X_s$  (16% and 17%). The moisture sources for these two regions are similar due to their proximity to extratropical Eurasia.

Second, the moisture sources are separated according to the atmospheric circulation and air mass. This separation is subjective; in previous studies, it varies from three to five sectors (Araguás-Araguás et al. 1998; Baker et al. 2015; Sun and Wang 2015; Chu et al. 2017; Jiang et al. 2017; Hu et al. 2018). Four sectors are used here, that is, the Eurasian Continent, the Indian Ocean, the Pacific Ocean, and the local region under study (Fig. 2, see the caption for details). The annual contributions from different sectors are listed in Table 2. The local contribution over the Tibetan Plateau (region 2, 26%) is much higher than other regions due to its topography. This is consistent with previous studies for similar regions using different methods (Guo et al. 2018; Zhang et al. 2017a; Curio et al. 2015).

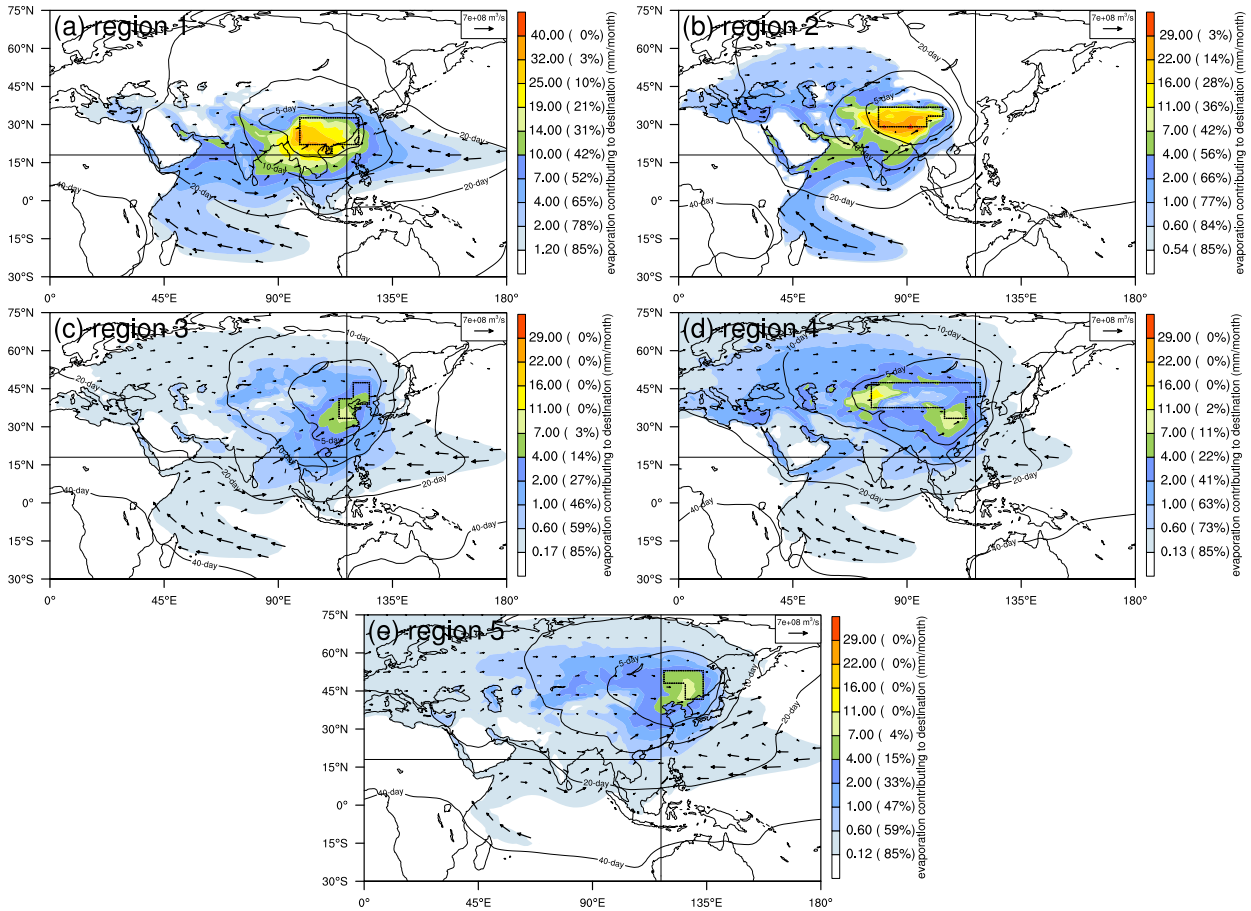


FIG. 2. (a)–(e) Annual mean tracked evaporation or moisture source (color) for five regions ( $\text{mm month}^{-1}$ ). Black boxes are the study regions. Vectors are the vertically integrated moisture flux ( $\text{m}^3 \text{s}^{-1}$ ). Contours are the atmospheric moisture traveling lifetime (day). Numbers in the parentheses along the color bar show the accumulated contribution of the tracked evaporation (beginning from the highest value of the tracked evaporation) to the annual regional precipitation. Contributions up to 85% are shown. Black lines in each panel divide the moisture sources into three sectors, the Pacific Ocean (to the right of the vertical black line), the Indian Ocean (to the left of the vertical black line and below the horizontal black line), and the Eurasian Continent (to the left of the vertical black line and above the horizontal black line). The target region is considered separately from any of the three aforementioned sectors.

The Eurasian Continent contribution increases with latitude. The Indian Ocean contribution decreases with latitude; the Pacific Ocean contribution decreases from east to west.

### b. Seasonal variations

Seasonal contributions (i.e., DJF, MAM, JJA, and SON) separated by land and sea as well as tropical and extratropical sources are listed in Table 1. Contributions from  $T_s$  are highest in JJA for all five regions, demonstrating the widespread impact of the EA summer monsoon, which is illustrated more directly in Fig. 3c (using JJA in region 1 as an example), showing the largest contributions from northern and equatorial Indian Ocean. Regions 1, 3, and 5 have larger contributions from  $T_s$  compared to other regions, indicating

the importance of the summer monsoon for controlling moisture for eastern EA. Contributions from  $X_l$  increase in MAM for all five regions. The largest contribution is over higher latitudes, indicating increased evaporation following the thaw of snow and frozen soil. For region 1, seasonal contributions are similar to the annual contributions, with  $T_s$  as the primary moisture source. For region 2, the similarity between seasonal and annual contributions is also maintained, with  $X_l$  as the primary moisture source. This similarity, however, breaks down over regions 3, 4, and 5 in DJF. These regions are dominated by extratropical sources throughout the year (66%, 85%, and 86%), but the contributions from  $X_s$  increase in DJF, while those of  $X_l$  decrease. For regions 3, 4, and 5, contributions from  $X_s$  (36%, 47%, and 60%) are

TABLE 1. Annual and seasonal moisture contributions separated into sea/land, tropics/extratropics, and local evaporation. The term  $T_s$  indicates moisture contribution from tropical sea,  $T_l$  is tropical land,  $X_s$  is extratropical sea,  $X_l$  is extratropical land, and  $\rho$  is the precipitation recycling ratio. The solstice latitudes (23.4°N and 23.4°S) are used to separate the tropics and extratropics. Annual (Ann) mean values are highlighted with bold font.

Region	Season	$T_s$	$T_l$	$X_s$	$X_l$	$\rho$
1	<b>Ann</b>	<b>50%</b>	<b>11%</b>	<b>8%</b>	<b>15%</b>	<b>16%</b>
	DJF	40%	14%	15%	17%	14%
	MAM	43%	15%	7%	21%	14%
	JJA	57%	10%	5%	12%	16%
	SON	47%	9%	12%	13%	19%
2	<b>Ann</b>	<b>24%</b>	<b>6%</b>	<b>7%</b>	<b>37%</b>	<b>26%</b>
	DJF	25%	10%	21%	31%	13%
	MAM	16%	4%	10%	40%	30%
	JJA	27%	6%	6%	37%	24%
	SON	27%	8%	5%	32%	28%
3	<b>Ann</b>	<b>28%</b>	<b>6%</b>	<b>11%</b>	<b>45%</b>	<b>10%</b>
	DJF	17%	9%	36%	29%	9%
	MAM	20%	8%	9%	54%	9%
	JJA	33%	6%	7%	44%	10%
	SON	19%	5%	22%	43%	11%
4	<b>Ann</b>	<b>12%</b>	<b>3%</b>	<b>16%</b>	<b>53%</b>	<b>16%</b>
	DJF	13%	5%	47%	30%	5%
	MAM	8%	3%	16%	56%	17%
	JJA	14%	3%	6%	57%	20%
	SON	12%	4%	24%	48%	12%
5	<b>Ann</b>	<b>12%</b>	<b>2%</b>	<b>17%</b>	<b>58%</b>	<b>11%</b>
	DJF	6%	2%	60%	25%	7%
	MAM	7%	2%	15%	64%	12%
	JJA	17%	3%	8%	60%	12%
	SON	7%	1%	31%	52%	9%

larger than those from  $X_l$  (29%, 30%, and 25%), becoming the primary moisture source in DJF.

The seasonal contributions from each sector are summarized in schematics (Fig. 4 and Table S1 in the online supplemental material). These contributions are further separated by moisture lifetime, as described in section 2. The same moisture lifetime contours (5, 10, and 20 days) are used in Fig. 4 (and Figs. S1–S4 in the online supplemental material) to allow the contributions from Fig. 4 to be mapped back onto geographic locations. For example, as mentioned previously, the moisture sources over the northern and equatorial Indian Ocean increase in JJA for region 1. Moisture originating from these regions travels for 10–20 days before precipitating within region 1. Therefore, a significant increase of moisture contribution from the Indian Ocean of 10–20 days lifetime in JJA is shown in Fig. 4a. For regions 4 and 5 in DJF (Figs. 4d,e), the moisture contributions from the Eurasian continent of 10–20 days lifetime are larger than from other sources. More specifically, moisture from Eurasia originates from eastern Europe and central Asia, which includes several water

TABLE 2. Annual moisture contributions separated into different sectors. Parameter  $\rho$  is the local contribution, EC is the Eurasian Continent, IO is the Indian Ocean, and PO is the Pacific Ocean.

Region	$\rho$	EC	IO	PO
1	16%	30%	37%	17%
2	26%	48%	24%	2%
3	10%	50%	20%	20%
4	16%	65%	12%	7%
5	12%	54%	9%	25%

bodies, for example, the Mediterranean Sea, Black Sea, Caspian Sea, and the northern part of the Persian Gulf. This is consistent with the result drawn from the land and sea separation, that is, for regions 4 and 5 in DJF, contributions from  $X_s$  dominate. Guo et al. (2018) found a significant negative relationship between the North Atlantic Oscillation (NAO) and the moisture flux entering regions 4 and 5. When the low-level westerly jet shifts southward over the midlatitude water bodies, the moisture flux to EA also increases. Further analysis of the link between the moisture sources and the NAO will be carried out in section 4b.

Seasonal cycles of the monthly  $\rho$  are shown in Fig. 5a. Although region 1 is the wettest region over EA, the contribution of local moisture is smaller than in other regions. During its wettest months, that is, June and July,  $\rho$  is smaller compared to that in the later months. This is because the EA summer monsoon circulation increases the convergence of moisture from remote sources. After the monsoon circulation retreats,  $\rho$  increases. A similar seasonal cycle is also seen over region 3, another region affected by the EA summer monsoon. The local moisture contribution over region 2 is larger than any other region throughout most the year. It dips during summer when the South Asian summer monsoon peaks. It also dips during winter, when local evaporation is small due to the frozen soil. Unlike the aforementioned regions, over region 4,  $\rho$  increases in summer but decreases in winter. Region 4 is a transition region between the wet and dry soil zones. Previous studies pointed out that, over such transition regions, local evaporation plays an important role in regulating local precipitation (Koster et al. 2004; Seneviratne et al. 2010). As evaporation increases in summer and decreases in the winter, so too does its contribution to local precipitation. A similar seasonal cycle is found over region 5. Seasonal cycles of  $\rho$  calculated using an analytic method (Guo et al. 2018) are compared to those from WAM-2layers in Fig. 5a. Both methods show similar seasonal variations, and the magnitudes of  $\rho$  are very similar over four regions, which shows the validity of both methods



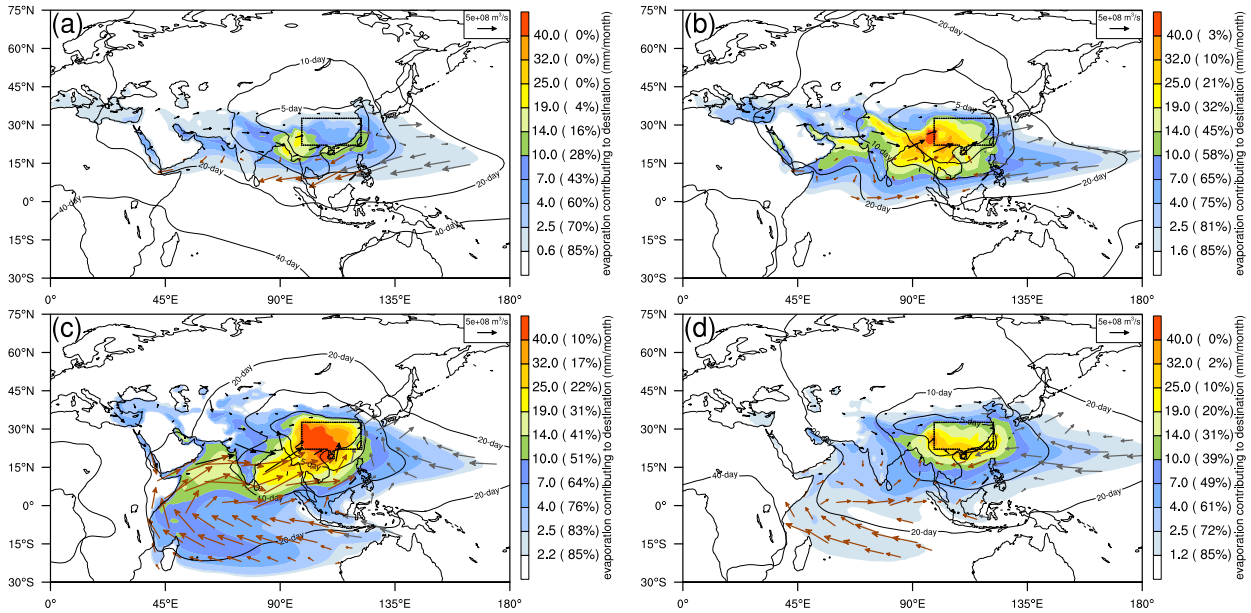


FIG. 3. As in Fig. 2, but for the seasonal mean moisture sources for region 1 for (a) DJF, (b) MAM, (c) JJA, and (d) SON.

for calculating moisture recycling. The largest discrepancy is over region 2, where  $\rho$  estimated from WAM-2layers is larger than that of the analytic method. The analytic method may underestimate  $\rho$  in this region, because the method is sensitive to moisture fluxes on the subjectively chosen boundary. Over a mountainous region such as region 2, setting the boundary on the windward side or the leeward side of the mountain can cause large differences in  $\rho$ . Using a different boundary, Curio et al. (2015) estimated  $\rho$  over the Tibetan Plateau to be as high as 63%.

Seasonal cycles of the area of the moisture source region are shown in Fig. 5b. The area of the moisture source region is defined as the area of the tracked evaporation that accounts for 85% of the precipitation in the target region. The seasonal cycles of the source area are anticorrelated with the seasonal cycles of the local moisture contribution (Fig. 5a). For example, with a greater local moisture contribution in region 2, the contributions from remote moisture are smaller, and so are the areas of these contributing regions. During the peak of the EA summer monsoon, the local moisture contribution decreases in regions 1 and 3, but the moisture from remote sources increases, as do the areas of the moisture source regions. The local evaporation over regions 4 and 5 decreases in the winter; correspondingly, the domains of the remote moisture source are enlarged. Not only does the contribution of local evaporation decrease in winter, but so does the evaporation from the entire Eurasian continent, which is the major moisture source for regions

4 and 5. As a result, moisture transported by the mid-latitude westerly jet originates further west, including the many inland water bodies as mentioned previously. These differences make the seasonal variations of the moisture source area over regions 1 and 3 (SE and CE of East Asia) oppose the seasonal variations over regions 4 and 5 (NW and NE of East Asia): moisture source area increases (decreases) in the summer but decreases (increases) in the winter for regions 1 and 3 (4 and 5).

#### 4. Interannual variation of moisture sources for EA precipitation

In this section, we investigate the interannual relationships between moisture sources, EA precipitation, and the atmospheric circulation.

##### a. Interannual variation of moisture sources with EA precipitation intensity

The 5-day atmospheric moisture lifetime contour is used here to determine the moisture source region. In the previous section, we used the perimeter of the tracked evaporation that accounts for 85% of EA precipitation to represent the domain of the moisture source. This change of approach is because, first, the domain of the tracked evaporation changes little on interannual time scales since the area enclosed is so large; second, using the moisture lifetime emphasizes interannual variations in the direction of moisture transport, and therefore the atmospheric circulation.

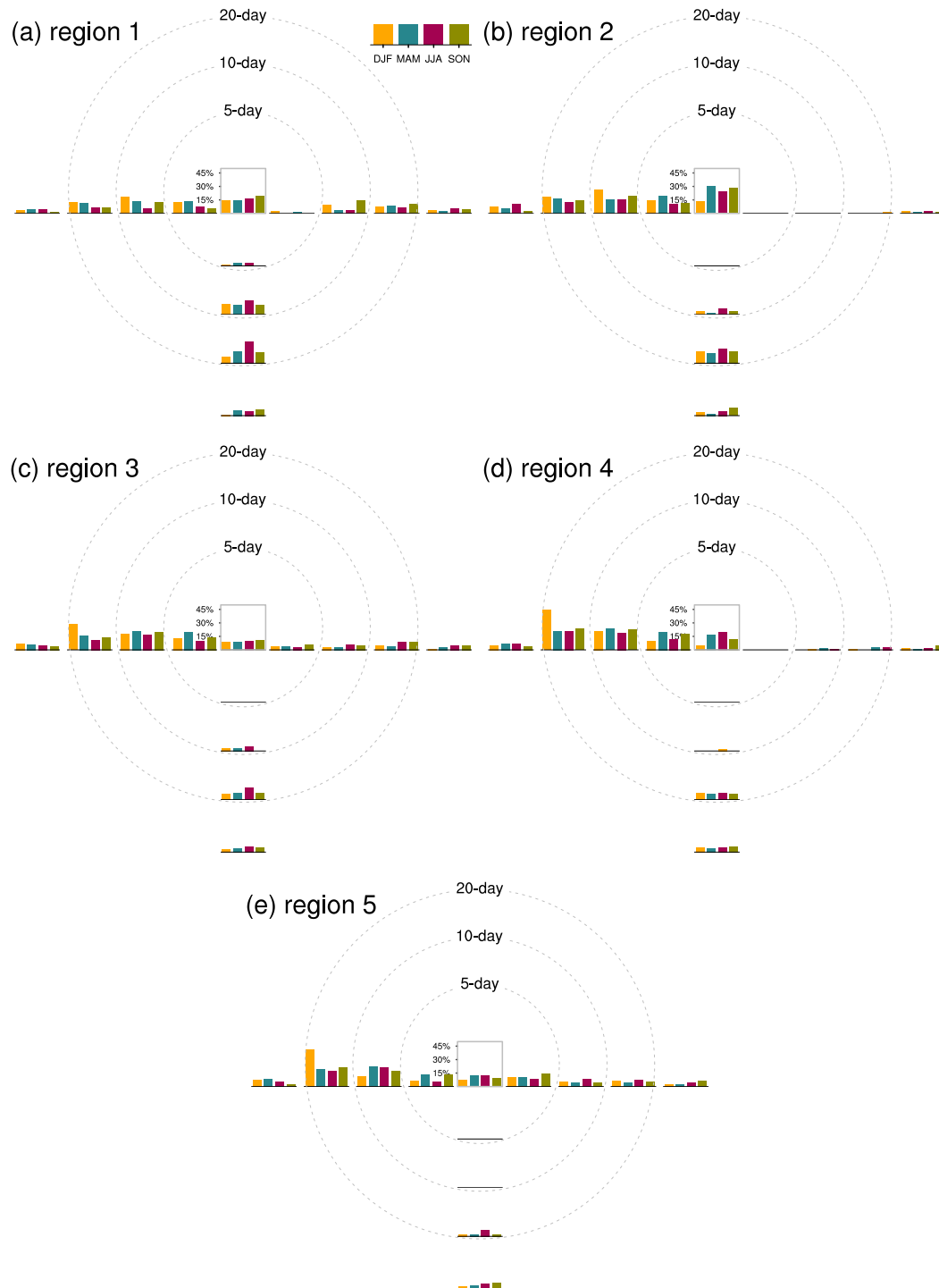


FIG. 4. (a)–(e) Seasonal moisture contributions from different sectors for five regions (%). Contributions are further divided by the moisture lifetime at values of 5, 10, and 20 days. The local moisture contribution is within the central box, the Eurasian continental contribution is on the left, the Pacific Ocean contribution is on the right, and the Indian Ocean contribution is on the bottom. Corresponding values on the plot can also be found in Table S1.

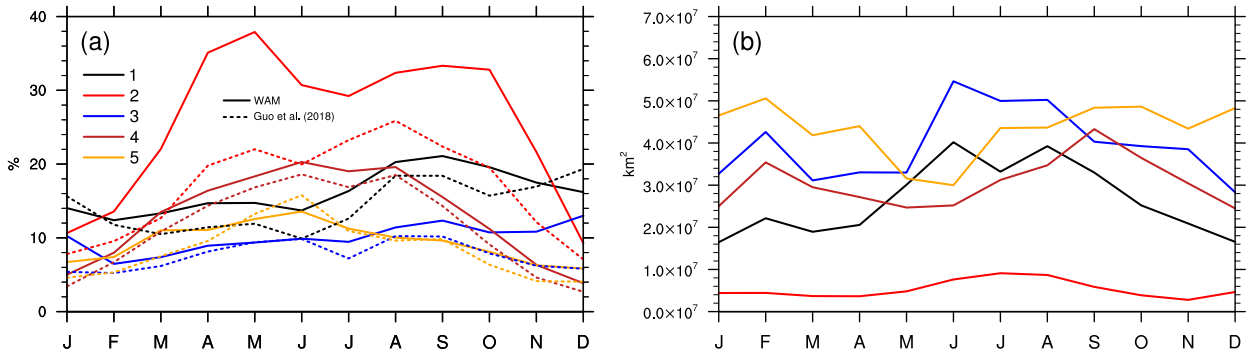


FIG. 5. (a) Seasonal cycles of the local moisture contribution for each region calculated from WAM-2layers (solid lines) and from the analytic method of Guo et al. (2018) (dotted lines; %). (b) Seasonal cycles of the area of the moisture source region that contributes 85% of precipitation over each region (km<sup>2</sup>).

Figure 6 shows the mean 5-day moisture lifetime contour for region 1 in DJF and region 3 in JJA, as well as the 5-day lifetime contours for the five wettest and driest seasons in the ERA-Interim record. The moisture source region clearly varies between the wettest and driest years. For region 1 in DJF in wet years, the moisture source shifts southeast to include more oceanic regions, indicating more moisture is obtained from the ocean. For region 3 in JJA in wet years, the moisture source shifts southwest but shifts northeast in dry years. As the anomalous moisture flux shows in Fig. 6b, the southwest shift in wet years is linked to southwesterly moisture flux anomalies, indicating a strong EA summer monsoon; the northeast shift in dry years, on the other hand, relates to northerly moisture flux anomalies indicative of a weak EA summer monsoon.

*b. Connection between moisture sources and circulation variability*

Previous studies have investigated the relationship between circulation variabilities and EA precipitation

(Zhou and Yu 2005; Li and Zhou 2012; Feng and Zhou 2012; Stephan et al. 2018; Guo et al. 2018). On the interannual time scale, Guo et al. (2018) found significant correlations between the NAO and westerly moisture influx to region 4 in DJF, and between ENSO and the southerly moisture influx of region 1. Based on these studies, in this section we investigate the NAO for region 4 (NW) in DJF, ENSO for region 1 (SE) in JJA, and the variation in the Somali Jet for region 2 (TP) in JJA. The NAO index is the time series of the leading empirical orthogonal function of sea level pressure anomalies over the Atlantic sector. This index is obtained from the Climate Data Guide (<http://climatedataguide.ucar.edu>). The ENSO index is the 3-month running mean of SST anomalies over the Niño-3.4 region. This index is obtained from the NOAA Climate Prediction Center (<http://origin.cpc.ncep.noaa.gov/>) and is calculated using the Extended Reconstructed Sea Surface Temperature v5. The Somali Jet index is a seasonal meridional wind measured at 850 hPa over 3°S–3°N, 40°–65°E. Similar metrics has been used in previous studies

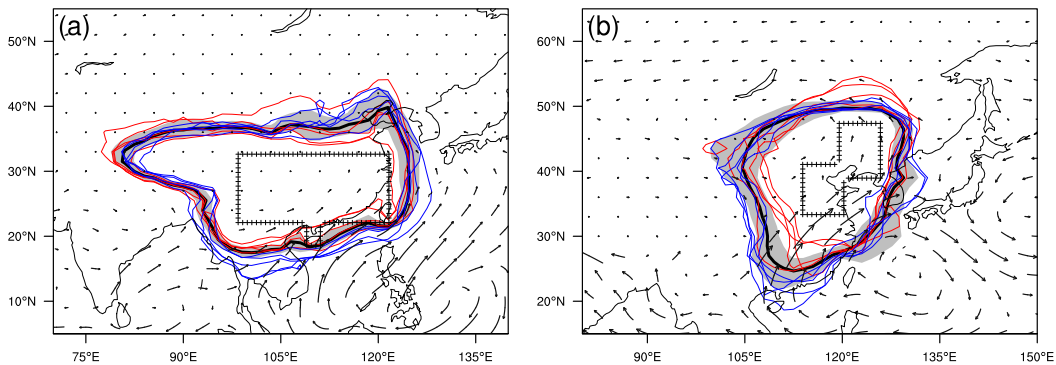


FIG. 6. Contours of 5-day moisture lifetime for (a) region 1 in DJF and (b) region 3 in JJA. The thick black line is the seasonal mean excluding the five wettest or driest years (1979–2015). The gray band indicates the range of the 5-day moisture lifetime (excluding the five wettest or driest years) between  $\pm\sigma$  (standard deviation). Thin blue lines are 5-day contours for the five wettest years. Thin red lines are 5-day contours for the five driest years. Vectors are the difference of the vertically integrated moisture flux (wet years minus dry years). The boxes show the regions under study.

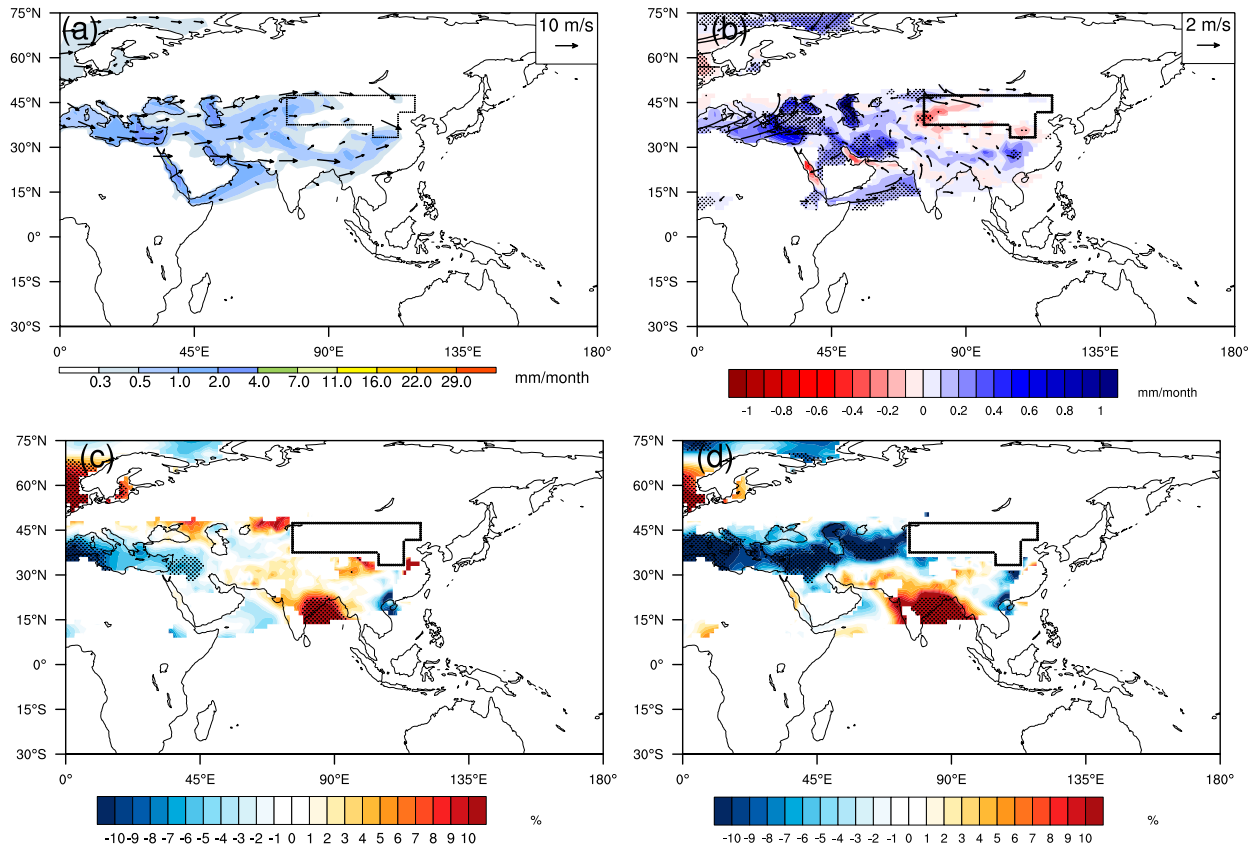


FIG. 7. (a) Tracked evaporation (color;  $\text{mm month}^{-1}$ ) and climatological 700-hPa wind (vector;  $\text{m s}^{-1}$ ) for region 4 in DJF. Changes in (b) the tracked evaporation ( $\text{mm month}^{-1}$ ) and wind ( $\text{m s}^{-1}$ ), (c) the traveling distance (%), and (d) the lifetime of moisture (%) between the negative and the positive NAO in DJF for region 4. Note that wind vectors in (a) and (b) are shown only within the region of tracked evaporation.

(e.g., Zhu 2012). Here, variations in the moisture source region and the properties of moisture along its trajectory (distance and lifetime) are investigated in conjunction with these circulation variabilities.

Figure 7a shows the mean moisture sources DJF precipitation for region 4. They are mainly over the midlatitude Eurasian continent including many inland water bodies, for example, the Mediterranean Sea and Caspian Sea. Differences between negative and positive NAOs (the DJF NAO indices with the normalized deviation of  $\leq -1$  and  $\geq 1$  are selected) are shown in Figs. 7b–d. In the negative NAO, the midlatitude westerlies are displaced southward over the Mediterranean Sea, from which more evaporation is transported to region 4 (Fig. 7b). This increased moisture from the source region during the negative NAO increases region 4 precipitation by 16%. Guo et al. (2018) also found that variations of moisture flux over the Eurasian continent explain most of the interannual precipitation variability in region 4 in DJF. These enhanced westerlies do not change the moisture traveling distance from the source

region to region 4 (Fig. 7c), which suggests the path of moisture transport does not change. However, the lifetime of moisture is shortened by as much as 10% (Fig. 7d), indicating that any change in the evaporation in the source region during the negative NAO has more rapid consequences for precipitation over region 4.

Figure 8a shows the mean moisture source JJA precipitation in region 1. The source region covers mainly the Indian Ocean and the western North Pacific Ocean. The low-level circulation over the equatorial Indian Ocean (via the Indian summer monsoon) and over the western North Pacific Ocean (via the subtropical high) are the major moisture pathways. Differences between the JJA seasons following El Niño and those following La Niña (the DJF Niño-3.4 indices in the previous winter of  $\geq 0.5^\circ\text{C}$  and  $\leq -0.5^\circ\text{C}$  are selected) are shown in Figs. 8b–d. It shows that the western North Pacific subtropical high is enhanced, but the Indian summer monsoon circulation is weakened (Fig. 8b). As a result, more moisture is transported to region 1 from the South China Sea, but less comes from the Indian Ocean

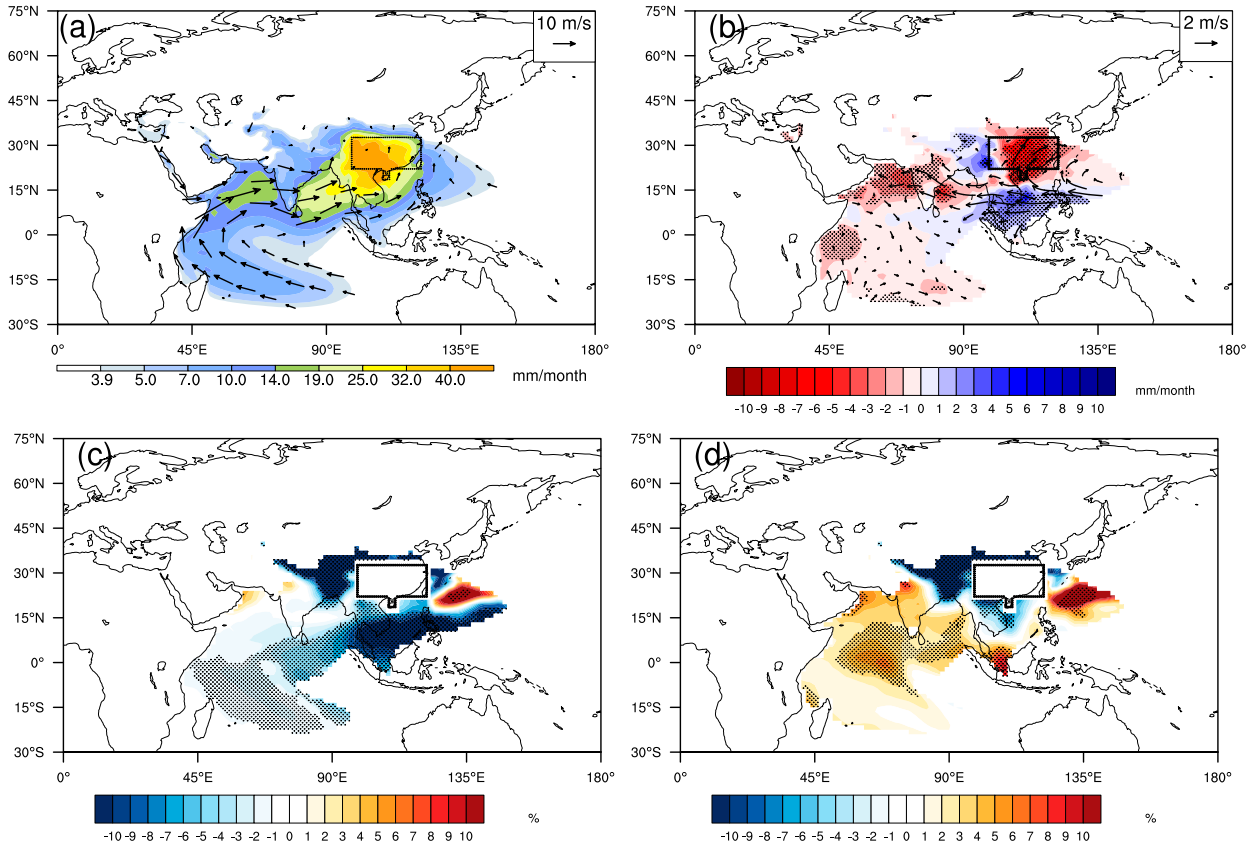


FIG. 8. (a) Tracked evaporation (color;  $\text{mm month}^{-1}$ ) and climatological 850-hPa wind (vector;  $\text{m s}^{-1}$ ) for region 1 in JJA. Changes in (b) the tracked evaporation ( $\text{mm month}^{-1}$ ) and wind ( $\text{m s}^{-1}$ ), (c) the traveling distance (%), and (d) the traveling lifetime (%) between JJAs trailing and preceding El Niño for region 1. Note that, the color scales of (a) and (b) are different from those in Fig. 7.

(Fig. 8b). This change in moisture sources results in mixed changes of precipitation in region 1, with increasing precipitation over the lower reaches of the Yangtze River, but decreasing precipitation over the southern coast of China, which is consistent with previous work (Zhang et al. 2017b). Changes in moisture traveling properties associated with ENSO, however, are different from those associated with the NAO. The traveling distance of moisture originating from the South China Sea is shortened, while the lifetime is not significantly changed (Figs. 8c,d). Over the low-latitude ocean (near 15°N), the anomalous circulation (easterly) opposes the mean circulation (westerly). This slows down the mean moisture transport from the Indian Ocean. On the other hand, the southerly anomaly conveys moisture more directly from the South China Sea to region 1 (Fig. 8b) instead being transported further east by the mean circulation (Fig. 8a). By combining these two changes, in JJAs following El Niño, moisture originating from the South China Sea and the Indo-China peninsula is transported more directly to region 1 but with a reduced speed,

which manifests as a decrease in traveling distance but no significant change in lifetime.

Figure 9a shows the mean moisture source for region 2 in JJA precipitation. Differences between strong and weak jet intensity (the normalized jet intensity anomalies of  $\geq 1$  and  $\leq -1$  are selected) are shown in Figs. 9b–d. The moisture sources vary according to the Somali Jet: in strong Somali Jet years, more moisture is transported to region 2 from the Indian Ocean (Fig. 9b), which increases region 2 precipitation by 9%. Changes in traveling properties are similar to those for the NAO, that is, the moisture lifetime is shortened in strong Somali Jet years, while the traveling distance changes little, suggesting little change in the shape of the circulation.

## 5. Discussion

### a. Choice of data

In this study, the ERA-Interim reanalysis is chosen as the single dataset to drive the Water Accounting Model-2layers (WAM-2layers). A comparison of moisture sources derived from WAM-2layers using different

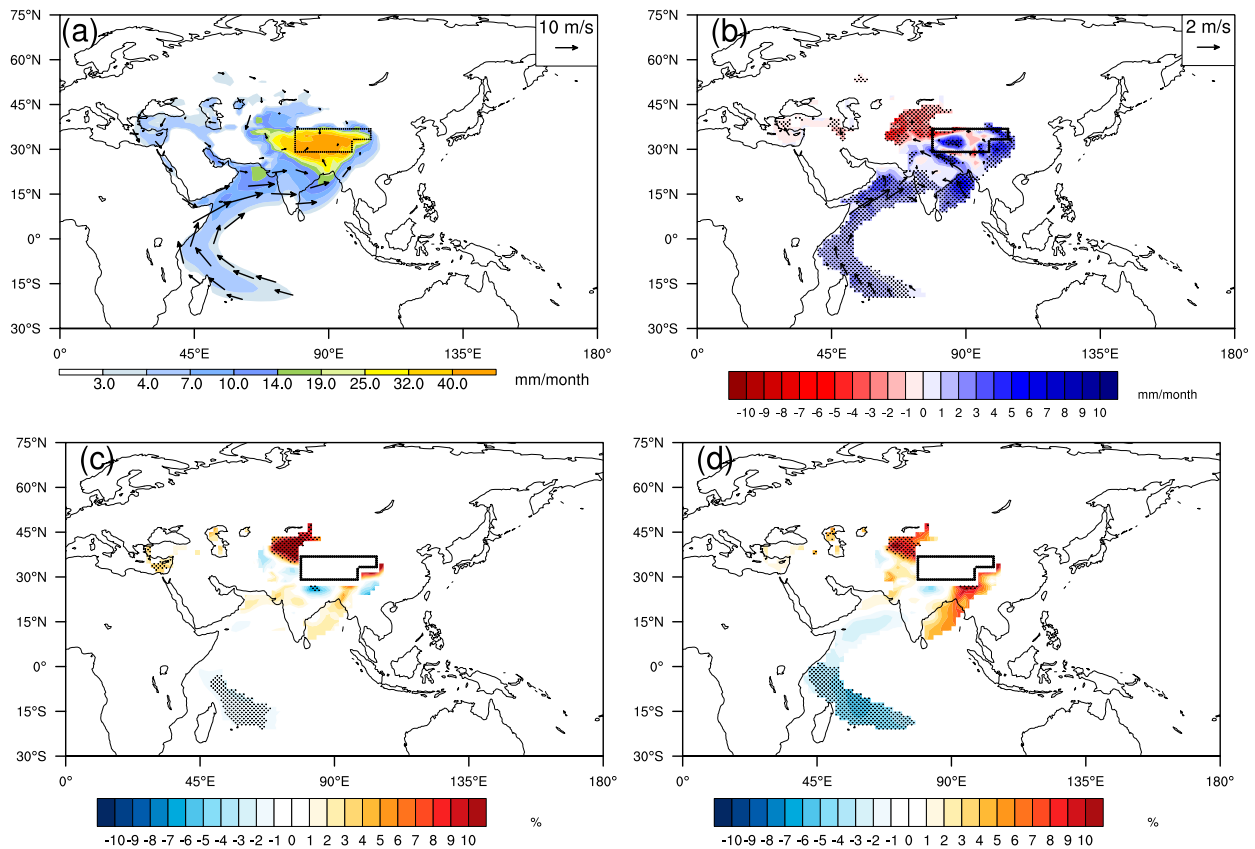


FIG. 9. (a) Tracked evaporation (color;  $\text{mm month}^{-1}$ ) and climatological 850-hPa wind (vector;  $\text{m s}^{-1}$ ) for region 2 in JJA. Changes in (b) the tracked evaporation ( $\text{mm month}^{-1}$ ) and wind ( $\text{m s}^{-1}$ ), (c) the traveling distance (%), and (d) the traveling lifetime (%) between the strong and the weak Somali Jet in JJA for region 2. Note that the color scales of (a) and (b) are different from those in Fig. 7.

reanalyses (ERA-Interim and Modern-Era Retrospective Analysis for Research and Applications) has been made by Keys et al. (2014). They compared moisture sources for northern China, the western Sahel, and the La Plata basin. They found a high level of agreement between these datasets in capturing the mean source regions, especially for northern China.

### b. Choice of method

We employed WAM-2layers (an Eulerian method) to analyze moisture sources for regional EA precipitation. WAM-2layers has the ability to track water from large areas with the same computational demand as from small areas.

Lagrangian methods are popular for tracing moisture sources for precipitation, likely because conventional Eulerian methods cannot track moisture from source to sink or vice versa, making it difficult to build a source-sink relationship for atmospheric moisture. However, for investigating moisture sources for precipitation over a large area and a long period, the computational resources required by Lagrangian methods can

be demanding. This is due to 1) the large number of infinitesimal air parcels required for the accuracy of Lagrangian methods; 2) the high temporal resolution of meteorological fields on three-dimensional grids; 3) the high frequency of the initiation of the tracking (e.g., 6 hourly); and 4) the requirement of an extra moisture source attribution scheme to convert millions of trajectories into a map of moisture source contributions. Note that, we refer mainly to three-dimensional Lagrangian methods here. There are existing two-dimensional Lagrangian methods that are more efficient, although at some expense to their accuracy (Hu and Dominguez 2015).

For these reasons, WAM-2layers is a more practical tool to conduct this study. However, several limitations of WAM-2layers need to be discussed. One limitation is the prescribed numerical dispersion, which could result in sources being more diffuse and further away than they are in reality. Another limitation affects locations with vertical wind shear. When the division between the upper and lower layers in WAM-2layers does not capture the actual vertical wind shear, the bias in moisture flux estimates could lead to biases in moisture tracking.

We also tested whether results in study are sensitive to noises due to model uncertainty or input data discrepancy by doing a sensitivity experiment. In this experiment, all input variables to WAM-2layers are given a small random perturbation. These random perturbations are sampled from a normal distribution with the mean of 0 and a standard deviation of 5% and are added to input variables on each time step. Changes in the tracked moisture source vary in the  $\pm 1\%$  range (figure not shown).

Comparisons between WAM-2layers and a 3D Lagrangian method (3D-Trajectories; Tuinenburg et al. 2012) for other regional and global domains can be found in van der Ent et al. (2013) and van der Ent and Tuinenburg (2017). These studies which show that these methods yield similar results.

### c. Other potential applications of WAM-2layers

Demory et al. (2014) showed simulated hydrological biases are associated with biases in the global and regional atmospheric circulation and in the energy budget. Sperber et al. (2013) showed that simulating EA summer monsoon precipitation remains challenging in state-of-the-art climate models. As WAM-2layers combines precipitation, evaporation and moisture fluxes into a single diagnosis via the atmospheric water conservation equation, it offers an integrated perspective for investigating precipitation biases in climate models. WAM-2layers could be more readily applied to model simulations, especially to the ever-growing set of model intercomparison projects (MIPs, for example, CMIP6) than many other moisture tracking methods, because WAM-2layers is less computationally demanding and requires only routine model output at modest frequencies. Although we used 6-hourly and 3-hourly data in the current study, we also tested daily data: the difference of tracked moisture sources between using daily and higher frequency data was less than  $\pm 5\%$ . WAM-2layers offers the ability to examine the sensitivity of the simulated hydrological cycle to various choices of model formulation, such as resolution and air–sea coupling.

In future climate projections, IPCC AR5 (Seneviratne et al. 2012) shows an uneven change in regional precipitation, with increases in the tropics and high latitudes and decreases in the subtropics and midlatitudes. Over EA, monsoon-related precipitation is projected to increase (Seneviratne et al. 2012). These changes will inevitably be associated with alterations in moisture sources for regional EA precipitation, however, the nature of these changes are unknown. Therefore, comparing moisture sources from future projections to those identified from present-day simulations will improve understanding and

confidence in projections of EA precipitation and water resource management in the future.

In this study, we focus on the mean and interannual time scale. However, changes on other time scales are also evident in the current results. For example, over the southeastern EA (region 1) in SON (Fig. 4a), the moisture contribution from the Pacific Ocean (28%) is higher than for any other season or region. This may be because there are more Pacific tropical cyclones making landfall over southeastern EA in SON. By comparing the moisture sources related to Pacific tropical cyclones to those related to the mean monsoon flow, previous studies showed that the contribution of tropical cyclones increases in SON as the EA summer monsoon retreats (Chen et al. 2010; Ren et al. 2006; Wang and Chen 2008; Wu et al. 2007; Guo et al. 2017). This is further supported by the fact that moisture that originates over the Pacific Ocean travels 5–10 days before precipitating over southeastern EA; the range of traveling time is in line with the lifetime of a tropical cyclone from its mature phase to landfall. Therefore, variations of moisture sources on other time scales should be investigated in the future.

## 6. Summary

We studied the moisture sources for annual and seasonal mean East Asia (EA) precipitation and its interannual variations. According to hydrological and topographic features, we divided EA into five regions: southeast, Tibetan Plateau, central east, northwest, and northeast. The moisture sources as well as its traveling properties (lifetime and distance) for each region were identified using WAM-2layers driven by ERA-Interim reanalysis for 1979–2015. The moisture traveling distance is a new tracer developed in this study for WAM-2layers.

The annual and seasonal mean moisture sources to regional precipitation were divided into the contributions from different sectors. First, the moisture sources were divided into tropical sea, tropical land, extratropical sea, and extratropical land. Alternatively, the moisture sources were divided into sectors according to origins over the Indian Ocean, the Pacific Ocean, the Eurasian continent, and the local region. In the annual mean, the tropical sea is the primary source for southeastern EA, but the extratropical land is the primary source for other regions. The contribution from local moisture is highest over the Tibetan Plateau. The contribution from the Indian Ocean decreases with latitude across EA, but the contribution from the Eurasian continent increases. The contribution from the Pacific Ocean decreases from east

to west across EA. In the seasonal mean, the EA monsoon circulation increases the moisture contribution from the tropical ocean during summer for all five regions. The contribution from extratropical land increases from winter to spring, indicating an increase in the availability of soil moisture for evaporation as the soil thaws. Over southeastern EA and the Tibetan Plateau, the primary contributors to the seasonal mean precipitation are similar to those for the annual mean. However, for the midlatitude regions (central-eastern, northwestern, and northeastern EA) in winter, the primary contributor to the seasonal mean differs from that to the annual mean; the contribution from the extratropical sea exceeds that from the extratropical land and becomes the primary contributor. The major source of this increasing extratropical ocean contribution is the inland water bodies over eastern Europe and central Asia (e.g., Mediterranean and Caspian Sea).

The local moisture contribution calculated using WAM-2layers is consistent with that from previous studies. It is highest over the Tibetan Plateau. The seasonal cycles of the local contribution differ among EA subregions. The local contribution peaks during the EA summer monsoon season in the northeastern and northwestern EA, but it peaks in the dry season in the southeastern and central-eastern EA. The seasonal cycle of the remote moisture contribution varies inversely to that of the local contribution. The size of the remote moisture source region for the Tibetan Plateau is smallest among EA subregions. The source area is larger for southeastern and central-eastern EA during summer. For northwest and northeast EA in winter, the source size is larger and covers the most of the Eurasian continent.

Interannual variations of the moisture source regions are linked to interannual circulation variations. For the negative NAO in DJF, more moisture is transported to northwestern EA by the stronger midlatitude westerly jet crossing the Eurasian continent. The stronger westerly reduces the moisture lifetime from source to sink, accelerating the regional hydrological cycle.

For JJA following El Niño, an anticyclonic circulation anomaly over the western North Pacific transports more moisture from the South China Sea to the southeastern EA. The more direct anomalous northward moisture flux from the South China Sea shortens the traveling distance from source to sink. On the other hand, the opposing directions of the anomalous circulation and the mean flow slow the transport of moisture. The combination of the shorter distance and the slower transport prevent any significant change in the moisture lifetime.

A stronger Somali Jet in JJA increases the moisture reaching the Tibetan Plateau and therefore also

the precipitation. The atmospheric lifetime of the moisture originating from the tropical Indian Ocean is significantly shortened.

*Acknowledgments.* This work and its contributors (LG, MED, PLV, AGT) were supported by the UK-China Research and Innovation Partnership Fund through the Met Office Climate Science for Service Partnership (CSSP) China as part of the Newton Fund. LG was also funded by the UK National Centre for Atmospheric Science Visiting Scientist Programme. RJE acknowledges the Innovational Research Incentives Scheme with project number 016.Veni.181.015, which is financed by the Netherlands Organisation for Scientific Research (NWO). RJE also acknowledges funding from the Netherlands Organization for Scientific Research (NWO), project number 016.Veni.181.015. NPK was also funded by a UK Natural Environment Research Council Independent Research Fellowship (NE/L010976/1).

#### REFERENCES

- Araguás-Araguás, L., K. Froehlich, and K. Rozanski, 1998: Stable isotope composition of precipitation over Southeast Asia. *J. Geophys. Res.*, **103**, 28 721–28 742, <https://doi.org/10.1029/98JD02582>.
- Baker, A. J., H. Sodemann, J. U. L. Baldini, S. F. M. Breitenbach, K. R. Johnson, J. van Hunen, and Z. Pingzhong, 2015: Seasonality of westerly moisture transport in the East Asian summer monsoon and its implications for interpreting precipitation  $\delta^{18}$ . *J. Geophys. Res. Atmos.*, **120**, 5850–5862, <https://doi.org/10.1002/2014JD022919>.
- Berrisford, P., and Coauthors, 2011: The ERA-Interim Archive: Version 2.0. ERA Rep. Series 1, 23 pp., <https://www.ecmwf.int/sites/default/files/elibrary/2011/8174-era-interim-archive-version-20.pdf>.
- Chen, J.-M., T. Li, and C.-F. Shih, 2010: Tropical cyclone- and monsoon-induced rainfall variability in Taiwan. *J. Climate*, **23**, 4107–4120, <https://doi.org/10.1175/2010JCLI3355.1>.
- Chu, Q., Q. Wang, and G. Feng, 2017: Determination of the major moisture sources of cumulative effect of torrential rain events during the pre-flood season over South China using a Lagrangian particle model. *J. Geophys. Res. Atmos.*, **122**, 8369–8382, <https://doi.org/10.1002/2016JD026426>.
- Curio, J., F. Maussion, and D. Scherer, 2015: A 12-year high-resolution climatology of atmospheric water transport over the Tibetan Plateau. *Earth Syst. Dyn.*, **6**, 109–124, <https://doi.org/10.5194/esd-6-109-2015>.
- Dee, D. P., and Coauthors, 2011: The ERA-Interim reanalysis: Configuration and performance of the data assimilation system. *Quart. J. Roy. Meteor. Soc.*, **137**, 553–597, <https://doi.org/10.1002/qj.828>.
- Demory, M.-E., P. L. Vidale, M. J. Roberts, P. Berrisford, J. Strachan, R. Schiemann, and M. S. Mizieliński, 2014: The role of horizontal resolution in simulating drivers of the global hydrological cycle. *Climate Dyn.*, **42**, 2201–2225, <https://doi.org/10.1007/s00382-013-1924-4>.
- Ding, Y., and J. C. L. Chan, 2005: The East Asian summer monsoon: An overview. *Meteor. Atmos. Phys.*, **89**, 117–142, <https://doi.org/10.1007/s00703-005-0125-z>.



- Feng, L., and T. Zhou, 2012: Water vapor transport for summer precipitation over the Tibetan Plateau: Multidata set analysis. *J. Geophys. Res.*, **117**, D20114, <https://doi.org/10.1029/2011JD017012>.
- Gong, D.-Y., and C.-H. Ho, 2002: The Siberian High and climate change over middle to high latitude Asia. *Theor. Appl. Climatol.*, **72**, 1–9, <https://doi.org/10.1007/s007040200008>.
- , S. W. Wang, and J. H. Zhu, 2001: East Asian winter monsoon and Arctic Oscillation. *Geophys. Res. Lett.*, **28**, 2073–2076, <https://doi.org/10.1029/2000GL012311>.
- Guo, L., N. P. Klingaman, P. L. Vidale, A. G. Turner, M.-E. Demory, and A. Cobb, 2017: Contribution of tropical cyclones to atmospheric moisture transport and rainfall over East Asia. *J. Climate*, **30**, 3853–3865, <https://doi.org/10.1175/JCLI-D-16-0308.1>.
- , —, M.-E. Demory, P. L. Vidale, A. G. Turner, and C. C. Stephan, 2018: The contributions of local and remote atmospheric moisture fluxes to East Asian precipitation and its variability. *Climate Dyn.*, **51**, 4139–4156, <https://doi.org/10.1007/s00382-017-4064-4>.
- Hu, H., and F. Dominguez, 2015: Evaluation of oceanic and terrestrial sources of moisture for the North American monsoon using numerical models and precipitation stable isotopes. *J. Hydrometeorol.*, **16**, 19–35, <https://doi.org/10.1175/JHM-D-14-0073.1>.
- Hu, Q., D. Jiang, X. Lang, and B. Xue, 2018: Moisture sources of the Chinese Loess Plateau during 1979–2009. *Palaeogeogr. Palaeoclimatol. Palaeoecol.*, **509**, 156–163, <https://doi.org/10.1016/j.palaeo.2016.12.030>.
- Huang, R., and Y. Wu, 1989: The influence of ENSO on the summer climate change in China and its mechanism. *Adv. Atmos. Sci.*, **6**, 21–32, <https://doi.org/10.1007/BF02656915>.
- Jiang, Z., S. Jiang, Y. Shi, Z. Liu, W. Li, and L. Li, 2017: Impact of moisture source variation on decadal-scale changes of precipitation in North China from 1951 to 2010. *J. Geophys. Res. Atmos.*, **122**, 600–613, <https://doi.org/10.1002/2016JD025795>.
- Keys, P. W., E. A. Barnes, R. J. van der Ent, and L. J. Gordon, 2014: Variability of moisture recycling using a precipitationshed framework. *Hydrol. Earth Syst. Sci.*, **18**, 3937–3950, <https://doi.org/10.5194/hess-18-3937-2014>.
- Koster, R. D., and Coauthors, 2004: Regions of strong coupling between soil moisture and precipitation. *Science*, **305**, 1138–1140, <https://doi.org/10.1126/science.1100217>.
- Li, X., and W. Zhou, 2012: Quasi-4-yr coupling between El Niño–Southern Oscillation and water vapor transport over East Asia–WNP. *J. Climate*, **25**, 5879–5891, <https://doi.org/10.1175/JCLI-D-11-00433.1>.
- , —, C. Li, and J. Song, 2013: Comparison of the annual cycles of moisture supply over southwest and southeast China. *J. Climate*, **26**, 10 139–10 158, <https://doi.org/10.1175/JCLI-D-13-00057.1>.
- Lin, R., T. Zhou, and Y. Qian, 2014: Evaluation of global monsoon precipitation changes based on five reanalysis datasets. *J. Climate*, **27**, 1271–1289, <https://doi.org/10.1175/JCLI-D-13-00215.1>.
- Pan, C., B. Zhu, J. Gao, and H. Kang, 2017: Source apportionment of atmospheric water over East Asia – A source tracer study in CAM5.1. *Geosci. Model Dev.*, **10**, <https://doi.org/10.5194/gmd-10-673-2017>.
- Ren, F., G. Wu, W. Dong, X. Wang, Y. Wang, W. Ai, and W. Li, 2006: Changes in tropical cyclone precipitation over China. *Geophys. Res. Lett.*, **33**, L20702, <https://doi.org/10.1029/2006GL027951>.
- Seneviratne, S. I., T. Corti, E. L. Davin, M. Hirschi, E. B. Jaeger, I. Lehner, B. Orlowsky, and A. J. Teuling, 2010: Investigating soil moisture–climate interactions in a changing climate: A review. *Earth Sci. Rev.*, **99**, 125–161, <https://doi.org/10.1016/j.earscirev.2010.02.004>.
- , and Coauthors, 2012: Changes in climate extremes and their impacts on the natural physical environment. *Managing the Risks of Extreme Events and Disasters to Advance Climate Change Adaptation*, C. B. Field et al., Eds., Cambridge University Press, 109–230.
- Simmonds, I., D. Bi, and P. Hope, 1999: Atmospheric water vapor flux and its association with rainfall over China in summer. *J. Climate*, **12**, 1353–1367, [https://doi.org/10.1175/1520-0442\(1999\)012<1353:AWVFAI>2.0.CO;2](https://doi.org/10.1175/1520-0442(1999)012<1353:AWVFAI>2.0.CO;2).
- Sperber, K. R., H. Annamalai, I.-S. Kang, A. Kitoh, A. Moise, A. Turner, B. Wang, and T. Zhou, 2013: The Asian summer monsoon: An intercomparison of CMIP5 vs. CMIP3 simulations of the late 20th century. *Climate Dyn.*, **41**, 2711–2744, <https://doi.org/10.1007/s00382-012-1607-6>.
- Stephan, C. C., N. P. Klingaman, P. L. Vidale, A. G. Turner, M.-E. Demory, and L. Guo, 2018: A comprehensive analysis of coherent rainfall patterns in China and potential drivers. Part I: Interannual variability. *Climate Dyn.*, **50**, 4405–4424, <https://doi.org/10.1007/s00382-017-3882-8>.
- Su, T., T. Feng, and G. Feng, 2015: Evaporation variability under climate warming in five reanalyses and its association with pan evaporation over China. *J. Geophys. Res. Atmos.*, **120**, 8080–8098, <https://doi.org/10.1002/2014JD023040>.
- Sun, B., and H. Wang, 2014: Moisture sources of semiarid grassland in China using the Lagrangian particle model FLEXPART. *J. Climate*, **27**, 2457–2474, <https://doi.org/10.1175/JCLI-D-13-00517.1>.
- , and —, 2015: Analysis of the major atmospheric moisture sources affecting three sub-regions of East China. *Int. J. Climatol.*, **35**, 2243–2257, <https://doi.org/10.1002/joc.4145>.
- Trenberth, K. E., J. T. Fasullo, and J. Mackaro, 2011: Atmospheric moisture transports from ocean to land and global energy flows in reanalyses. *J. Climate*, **24**, 4907–4924, <https://doi.org/10.1175/2011JCLI4171.1>.
- Tuinenburg, O. A., R. W. A. Hutjes, and P. Kabat, 2012: The fate of evaporated water from the Ganges basin. *J. Geophys. Res.*, **117**, D01107, <https://doi.org/10.1029/2011JD016221>.
- van der Ent, R. J., and O. A. Tuinenburg, 2017: The residence time of water in the atmosphere revisited. *Hydrol. Earth Syst. Sci.*, **21**, 779–790, <https://doi.org/10.5194/hess-21-779-2017>.
- , H. H. G. Savenije, B. Schaefli, and S. C. Steele–Dunne, 2010: Origin and fate of atmospheric moisture over continents. *Water Resour. Res.*, **46**, W09525, <https://doi.org/10.1029/2010WR009127>.
- , O. A. Tuinenburg, H.-R. Knoche, H. Kunstmann, and H. H. Savenije, 2013: Should we use a simple or complex model for moisture recycling and atmospheric moisture tracking? *Hydrol. Earth Syst. Sci.*, **17**, 4869–4884, <https://doi.org/10.5194/hess-17-4869-2013>.
- , L. Wang-Erlandsson, P. W. Keys, and H. H. G. Savenije, 2014: Contrasting roles of interception and transpiration in the hydrological cycle – Part 2: Moisture recycling. *Earth Syst. Dyn.*, **5**, 471–489, <https://doi.org/10.5194/esd-5-471-2014>.
- Wang, S.-Y., and T.-C. Chen, 2008: Measuring East Asian summer monsoon rainfall contributions by different weather systems over Taiwan. *J. Appl. Meteor. Climatol.*, **47**, 2068–2080, <https://doi.org/10.1175/2007JAMC1821.1>.
- Wang, B., R. Wu, and X. Fu, 2000: Pacific–East Asian teleconnection: How Does ENSO affect East Asian climate? *J. Climate*, **13**, 1517–1536, [https://doi.org/10.1175/1520-0442\(2000\)013<1517:PEATHD>2.0.CO;2](https://doi.org/10.1175/1520-0442(2000)013<1517:PEATHD>2.0.CO;2).
- , —, and T. Li, 2003: Atmosphere–warm ocean interaction and its impacts on Asian–Australian monsoon variation. *J. Climate*, **16**, 1195–1211, [https://doi.org/10.1175/1520-0442\(2003\)16<1195:AOIAII>2.0.CO;2](https://doi.org/10.1175/1520-0442(2003)16<1195:AOIAII>2.0.CO;2).

- Wei, J., P. A. Dirmeyer, M. G. Bosilovich, and R. Wu, 2012: Water vapor sources for Yangtze River Valley rainfall: Climatology, variability, and implications for rainfall forecasting. *J. Geophys. Res.*, **117**, D05126, <https://doi.org/10.1029/2011JD016902>.
- Wu, B., T. Li, and T. Zhou, 2010: Relative contributions of the Indian Ocean and local SST anomalies to the maintenance of the western North Pacific anomalous anticyclone during the El Niño decaying summer. *J. Climate*, **23**, 2974–2986, <https://doi.org/10.1175/2010JCLI3300.1>.
- Wu, Y., S. Wu, and P. Zhai, 2007: The impact of tropical cyclones on Hainan Island's extreme and total precipitation. *Int. J. Climatol.*, **27**, 1059–1064, <https://doi.org/10.1002/joc.1464>.
- Xie, S.-P., K. Hu, J. Hafner, H. Tokinaga, Y. Du, G. Huang, and T. Sampe, 2009: Indian Ocean capacitor effect on Indo-western Pacific climate during the summer following El Niño. *J. Climate*, **22**, 730–747, <https://doi.org/10.1175/2008JCLI2544.1>.
- Zhai, P., X. Zhang, H. Wan, and X. Pan, 2005: Trends in total precipitation and frequency of daily precipitation extremes over China. *J. Climate*, **18**, 1096–1108, <https://doi.org/10.1175/JCLI-3318.1>.
- Zhang, C., Q. Tang, and D. Chen, 2017a: Recent changes in the moisture source of precipitation over the Tibetan Plateau. *J. Climate*, **30**, 1807–1819, <https://doi.org/10.1175/JCLI-D-15-0842.1>.
- Zhang, R., Q. Min, and J. Su, 2017b: Impact of El Niño on atmospheric circulations over East Asia and rainfall in China: Role of the anomalous western North Pacific anticyclone. *Sci. China Earth Sci.*, **60**, 1124–1132, <https://doi.org/10.1007/s11430-016-9026-x>.
- Zhao, T., J. Zhao, H. Hu, and G. Ni, 2016: Source of atmospheric moisture and precipitation over China's major river basins. *Front. Earth Sci.*, **10**, 159–170, <https://doi.org/10.1007/s11707-015-0497-4>.
- Zhou, T.-J., and R.-C. Yu, 2005: Atmospheric water vapor transport associated with typical anomalous summer rainfall patterns in China. *J. Geophys. Res.*, **110**, D08104, <https://doi.org/10.1029/2004JD005413>.
- Zhu, Y., 2012: Variations of the summer Somali and Australia cross-equatorial flows and the implications for the Asian summer monsoon. *Adv. Atmos. Sci.*, **29**, 509–518, <https://doi.org/10.1007/s00376-011-1120-6>.